Review Article **Open Access**

Andrew Shamp and Eva Zurek*

Superconductivity in Hydrides Doped with Main Group Elements Under Pressure

DOI 10.1515/nsm-2017-0003
Received November 5, 2016; accepted January 18, 2017

Abstract: *A priori* crystal structure prediction techniques have been used to explore the phase diagrams of hydrides of main group elements under pressure. A number of novel phases with the chemical formulas MH_n, $n > 1$ and M = Li, Na, K, Rb, Cs; MH_n, $n > 2$ and M= Mg, Ca, Sr, Ba; H_nI with $n > 1$ and PH, PH_2, PH_3 have been predicted to be stable at pressures achievable in diamond anvil cells. The hydrogenic lattices within these phases display a number of structural motifs including $H_2^{\delta-}$, H^-, H_3^-, as well as one-dimensional and three-dimensional extended structures. A wide range of superconducting critical temperatures, T_cs, are predicted for these hydrides. The mechanism of metallization and the propensity for superconductivity are dependent upon the structural motifs present in these phases, and in particular on their hydrogenic sublattices. Phases that are thermodynamically unstable, but dynamically stable, are accessible experimentally. The observed trends provide insight on how to design hydrides that are superconducting at high temperatures.

Keywords: superconductivity, hydrides, high pressure, density functional theory, materials prediction

1 Introduction

In a seminal work Ashcroft proposed that because the hydrogen is "chemically precompressed" in solids composed of the group 14 hydrides, less physical pressure would be required to metallize them as compared to pure hydrogen [1, 2]. Moreover, he hypothesized that these phases have the potential to be superconducting at high temperatures. Ashcroft's predictions led to a plethora of theoretical, and a few experimental, studies that searched for superconductivity in hydrides that are known to exist at atmospheric conditions, such as SiH_4 [3–10], GeH_4 [11–14], and AlH_3 [15–17]. He also pointed out that a second component, which can be seen as an impurity, may potentially reduce the pressure required to metallize hydrogen [18].

Pressure can affect which combinations of elements form stable phases, and the chemical compositions of these phases. Therefore, building on Ashcroft's proposals, density functional theory (DFT) calculations were carried out to predict the structures of hydrides with stoichiometries that are not stable at atmospheric conditions, in the hopes of uncovering hitherto unknown superconductors [19]. Since then, numerous theoretical studies have been performed that investigate the phase diagrams of hydrogen doped with the electropositive alkali metals or alkaline earth metals [20–34], as well as the electronegative element iodine [35, 36] under pressure. Experimental work on the hydrides of lithium and sodium confirmed that species with unique stoichiometries such as NaH_3 and NaH_7 can be synthesized in diamond anvil cells, but the phases that have been reported to date do not exhibit superconductivity [21, 37]. Nonetheless, as summarized in this short review, the aforementioned theoretical explorations have: revealed that rich structural variety may be found in the hydrogenic sublattices, suggested a number of ways that hydrogen may be metalized via doping, and shown that the propensity for superconductivity is linked to the nature of the hydrogenic motifs.

Recent experimental studies carried out by Drozdov, Eremets, and Troyan on hydrides containing a *p*-block element have yielded exciting results. It was shown that when hydrides of sulfur were prepared at $T \geq 300$ K they become superconducting with a critical temperature, T_c, of 203 K at 150 GPa [38], and at 207 GPa compressed phosphine yielded a T_c of 103 K [39]. Theoretical studies, which have shown that the superconductivity observed in Ref. [38] arises primarily from an H_3S phase [40–55] whose structure has been recently confirmed experimentally [56], will not be described within this short review. We will, however, discuss the results of first principles calculations carried out for the hydrides of phosphorus [57–59]. Importantly, these studies revealed that the phases made in experiment are not necessarily the thermodynamic minima,

Andrew Shamp: Department of Chemistry, State University of New York at Buffalo, Buffalo, NY 14260-3000, USA
***Corresponding Author: Eva Zurek:** Department of Chemistry, State University of New York at Buffalo, Buffalo, NY 14260-3000, USA, E-mail: ezurek@buffalo.edu

and that a mixture of phases could yield the observed superconductivity.

These studies highlight that new hydrogen-rich materials, some of which may have a T_c higher than those previously thought possible for Bardeen-Cooper-Schrieffer (BCS)-type superconductors, can be attained under pressure, and they have reinvigorated the search for high-temperature superconductivity in high-pressure hydrides.

2 How to Metallize with an Electropositive Element

A number of chemical trends have been observed for compressed alkali metal and alkaline earth polyhydrides [33]. The pressure at which the polyhydrides were calculated to become stable with respect to decomposition into the "classic" hydride (of MH or MH_2 stoichiometry) and H_2 decreases with decreasing ionization potential of the dopant metal. For example, whereas LiH_n phases are thermodynamically stable above 100 GPa, CsH_n structures are accessible above 2 GPa. The stoichiometries of the thermodynamically stable polyhydrides, eg. those which comprised the convex hull, possessed an odd number of hydrogen atoms if the dopant atom was from Group I, and an even number it was from Group II. The only exception to this trend was lithium, wherein LiH_2, LiH_6, and LiH_8 were found to be thermodynamically stable. In general, past a threshold pressure the hydrogen content in the structure with the most negative enthalpy of formation, ΔH_F, decreased with increasing pressure for the alkali metal polyhydrides, whereas for the alkaline earth polyhydrides it increased. Thus, it is likely that at very high pressures the mole % ratio of hydrogen found in the structure that corresponds to the lowest point on the convex hull will be larger in the alkaline earth polyhydrides than in the alkali metal polyhydrides.

Whereas "chemical precompression" can be employed to metallize *covalent* hydrides at pressures lower than those required for elemental hydrogen, different ways to metallize become important for *ionic* hydrides. We have found five mechanisms that hasten band gap closure, and four of these are explicitly illustrated schematically in Fig. 1. Which route is taken depends upon the nature of the hydrogenic motifs present in the lattice, and this in turn is governed by the nature of the dopant element. In the paragraphs that follow these five approaches are described by way of example.

1. In the phases that contained only hydrogen molecules, such as $R\bar{3}m$-LiH_6 shown in Fig. 1(a), valence electrons are transferred from the electropositive metal to the H_2 σ_u^*-orbitals, which become partially filled [19]. As a consequence, these systems are already good metals at 1 atm (but they are not stable). This mechanism of metallization yields phases with a high density of states (DOS) at the Fermi level, E_F.

2. At 1 atm the volume of the $R\bar{3}m$-LiH_6 unit cell was calculated to be a factor of two smaller than an optimized H_6 lattice because ionic attraction between Li^+ and three $(H_2)^{-1/3}$ molecules leads to "Madelung precompression". However, this method of precompression was only effective at low pressures because the presence of the Li^+ core yielded a structure with a volume larger than that of elemental H_2 at high pressures. Therefore, this metallization mechanism is likely only effective for ionic compounds that undergo pressure-induced band gap closure at relatively low pressures.

3. The valence electrons of the electropositive element can be transferred to a single hydrogen atom yielding a hydridic hydrogen, H^-, within a lattice of H_2 molecules, as in the Pm-NaH_9 structure illustrated in Fig. 1(b) [26]. Because an H^- impurity donor band forms between the H_2 σ_g- and σ_u^*-levels, the band gap of this system is smaller at 1 atm than in elemental H_2. Therefore, phases possessing H^- should undergo metallization due to band broadening and overlap at lower pressures than those required to metallize pure hydrogen. However, calculations have shown that the DOS at E_F in the metalized systems is generally quite low.

It has been proposed that the formation of H^- vs. $H_2^{\delta-}$ molecules depends upon the number of formal "effectively added electrons" donated from the electropositive element to the hydrogenic sublattice [22]. Because these electrons fill the antibonding σ_u^*-orbitals in H_2, the H–H bond elongates. If the filling is large enough (for example because the H:M ratio is low) this bond is expected to break, forming hydridic hydrogens.

4. Because H^- is a soft base it can interact with H_2, an extremely weak acid, to form H_3^-, the simplest example of a three–center four–electron (3c-4e) bond. Calculations carried out with a variant of the configuration interaction (CI) method have shown that H_3^- is asymmetric with H–H distances measuring 0.75 and 2.84 Å, and the barrier between the two possible minima is symmetric, with H–H distances measuring ~1.06 Å [60]. Symmetric and asymmetric H_3^- motifs have been observed in polyhydrides containing Na [21], K [28], Rb [27], Cs [29], Sr [23, 32] and Ba [31]: one example is the RbH_5 phase illustrated in Fig. 1(c) [27]. In these species metallization occurs via the pressure induced broadening and eventual overlap of the filled H_3^- non-bonding band with the H_3^- anti-bonding bands and/or

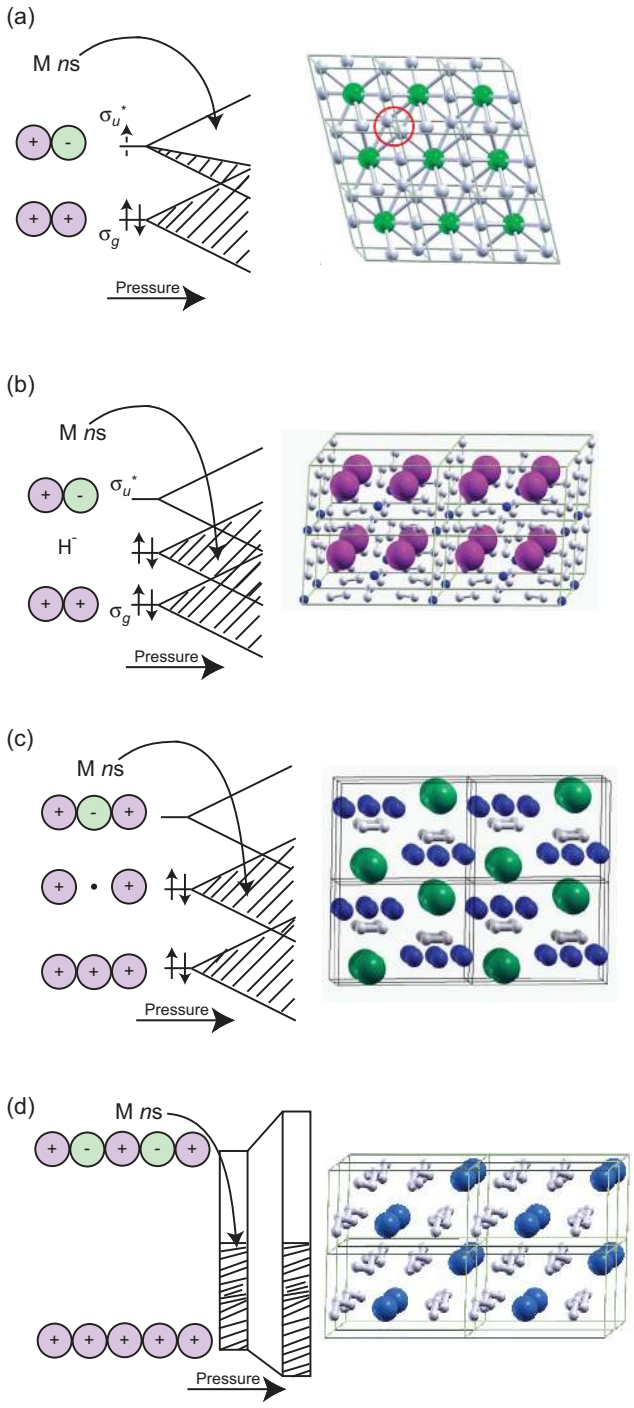

Figure 1: Schematic illustrations of the mechanisms by which polyhydrides doped with an electropositive element can metallize. (a) Partial filling of the σ_u^*-band (the dashed arrow denotes occupation by a fraction of an electron), as in LiH_6 [19]. (b) Introduction of an "impurity band" of H^- between the σ_g- and σ_u^*-bands, and pressure induced overlap, as in NaH_9 [26]. (c) Pressure induced overlap of the non-bonding and anti-bonding H_3^- bands, as in RbH_5 [27]. (d) Formation of a one-dimensional hydrogenic chain, as in SrH_6 [32]. These mechanisms occur in hydrogenic sublattices that contain the following hydrogenic motifs: (a) only $H_2^{\delta-}$, (b) H^-, (c) H_3^-, (d) $\frac{1}{\infty}[H^{\delta-}]$. "Madelung precompression" may occur for any of these lattices in the low pressure regime.

the metal *d*-bands. As a result, the DOS at E_F in the metallic phases is typically low.

The M^+–H^- interaction decreases the basicity of the hydride, so the formation of H_3^- is easiest in the gas phase, followed by the polyhydride containing the softest metal cation [28]. This explains why H_3^- units were not observed in the polyhydrides of lithium, magnesium and calcium. Under pressure the H_3^- motif tends to symmetrize in many of the structures that were found, and both bent and linear units have been observed.

5. Perhaps the most important mechanism of metallization was found to occur in only a few phases, for example CaH_6 above 150 GPa [22] and the $R\bar{3}m$-SrH_6 structure shown in Fig. 1(d) [23, 32]. All of the hydrogens within these systems were partially negatively charged, $H^{\delta-}$, and they were close enough for their electron densities to overlap and form extended lattices. In CaH_6 the hydrogenic lattice was three-dimensional and resembled the framework of the sodalite clathrate, whereas in SrH_6 the hydrogen atoms formed one-dimensional hydrogenic helices, $\frac{1}{\infty}[H^{\delta-}]$. The presence of the extended hydrogenic lattices gave rise to metallicity in these phases, and yielded a high DOS at E_F. Calculations have predicted that hydrogenic sodalite-like lattices will also be found in MgH_6 around 260 GPa [34] and YH_6 at 120 GPa [61].

3 Metallization in the Presence of *p*-Block Elements

Many of the known hydrides of a *p*-block element form covalent bonds with hydrogen, so they can hasten its metallization by "chemical precompression". In this section we show that the non-hydrogenic lattice can be important for the metallization of an ionic hydride containing a *p*-block element wherein the hydrogen is the more electropositive species. And, metastable covalent hydrides composed of one-dimensional chains or two-dimensional layers that have nearly free electron like behavior are described.

1. All of the strategies that can be utilized to accelerate band gap closure via doping hydrogen with an electronegative element involve metallizing the hydrogenic sublattice. However, theoretical investigations of H_nI, $n > 1$, revealed that it is not only the hydrogenic sublattice which is important for inducing metallization [35].

The stable polyhydrides of iodine contained the following structural motifs: $I^{\delta+}$, $H^{\delta+}$, and $H_2^{\delta-}$ molecules as in H_5I, or $I^{\delta+}$ and $H_2^{\delta-}$ molecules as in H_2I and H_4I; these phases are illustrated in Fig. 2 [35]. The former could be thought of as a HI lattice with excess H_2 molecules, whereas the latter two consisted of an atomistic iodine

host lattice within which H_2 molecules were guests. The metallic behavior of these phases was found to originate from the HI or iodine sublattices. Atomistic hydrogen was present in a $R\bar{3}m$-H_2I phase at 246 GPa [36].

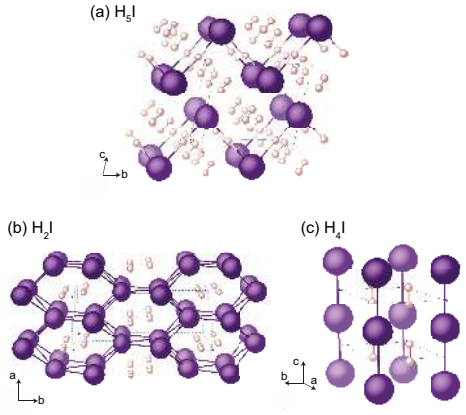

Figure 2: Supercells of (a) $P1$-H_5I, (b) $Cmcm$-H_2I and (c) $P6/mmm$-H_4I from Ref. [35].

The $P1$ symmetry H_5I phase shown in Fig. 2(a) was stable between 50-90 GPa. It contained zigzag $[HI]_\infty$ chains within which every iodine atom was bound to two hydrogen atoms. The H–I distances were nearly equivalent, indicative of multi-center bonding. This zigzag structural motif, and the equalization of inter- and intra-molecular H-X bonds under pressure, occurs in the halogen hydrides with traditional stoichiometries, HX (X=F, Cl, Br) [62]. H_2 molecules bearing a slight negative charge surrounded the hydrogens comprising the $[HI]_\infty$ chains in H_5I.

Experiments have shown that HI undergoes a pressure induced insulator to metal transition below 50 GPa [63]. At this pressure the PBE band gap of H_5I was calculated to be ∼0.5 eV. By 65 GPa H_5I became metallic, however it is well known that the PBE functional underestimates the pressure at which band gap closure occurs. The metallization of H_5I is a result of the pressure induced broadening of the valence band, primarily of iodine p-character, and the conduction band, exhibiting mainly $H^{\delta+}$ s-character, and the system had a low DOS at E_F. Thus, the mechanism of metallization is the same in H_5I and HI, but because the volume of the former is larger at a given pressure than that of the latter (due to the excess H_2 molecules), higher pressures are required to metallize the polyhydride.

The $Cmcm$-H_2I and $P6/mmm$-H_4I phases illustrated in Fig. 2(c,d) lay on the 100, 150, and 200 GPa convex hulls. H_2I consisted of a three-dimensional iodine lattice with two rows of H_2 molecules arranged in a zigzag fashion that run through channels formed by the iodine host. H_4I

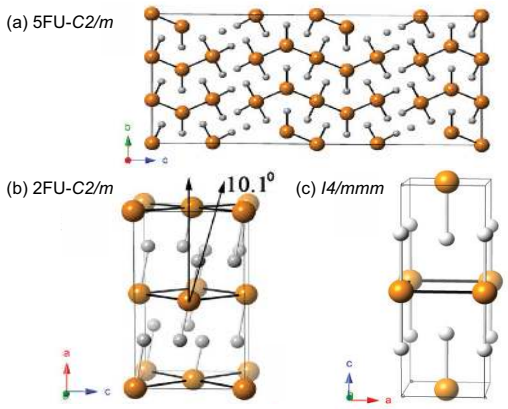

Figure 3: Supercells of (a) 5FU-$C2/m$ PH_2, (b) 2FU-$C2/m$ PH_2 and (c) $I4/mmm$ PH_2 from Ref. [57].

was composed of parallel one-dimensional chains of iodine atoms and H_2 molecules. In both phases there was a slight transfer of charge from iodine to H_2. These systems were good metals already at 1 atm, even though they were not thermodynamically or dynamically stable at this pressure. The high DOS at E_F was primarily due to iodine p-states, with an admixture of hydrogen s.

Within elemental iodine, pressure causes the I–I bonds to stretch, and the intermolecular distances to decrease. At ∼16 GPa iodine undergoes an insulator to metal transition [64], and by 30 GPa a monoatomic metallic phase forms wherein the I–I distances are equalized [65]. Thus, the metallicity within H_2I and H_4I originates from the fact that their iodine sublattices are atomistic. Single point calculation on these geometries at 100 GPa, but where the hydrogens were removed, illustrated that they were metallic. Interestingly, the DOS at E_F of the iodine lattices alone was slightly higher than that of the iodine polyhydrides. Whereas the H_2 lattice of H_2I was insulating, the one for H_4I had a small, but non-negligible DOS at E_F.

2. Recently, Drozdov, Eremets, and Troyan observed superconductivity in phosphine, PH_3, which was liquefied and compressed in a diamond anvil cell [39]. The T_c was measured to be 30 K at 83 GPa and 103 K at 207 GPa via resistance measurements. Because PH_3 is a covalent hydride at atmospheric conditions, the hydrogen within it is "chemically precompressed".

Three different groups nearly simultaneously studied the phase diagram of PH_n, $n = 1-6$, at these pressures via first principles calculations [57–59]. These studies found that even though the phosphine polyhydrides are unstable with respect to decomposition into solid phosphorus and H_2 at the pressures considered experimentally, a number of phases were dynamically stable. Many of the structures that were identified via *a priori* crystal structure pre-

diction techniques consisted of one-dimensional chains or two-dimensional layers wherein the environment around the phosphorus atoms resembled that in the hypervalent PCl_5 or PCl_6^- molecules. Typically, the phosphorus atoms were octahedrally coordinated to phosphorus and hydrogen atoms, but in some structures trigonal bipyramidal coordination was observed.

Consider, for example, the three PH_2 phases illustrated in Fig. 3 that had nearly the same (non-zero-point corrected) enthalpies at 150 GPa. A $C2/m$ symmetry structure with five formula units in the primitive cell, 5FU-$C2/m$ PH_2, consisted of PH_3-PH-PH_2-PH-PH_3 oligomers that were 1D periodic along the a-axis. Whereas the terminal and central phosphorus atoms in this phase were octahedrally coordinated, the phosphorus atoms within the -PH- segment were nearly trigonal bipyramidal. The phosphorus atoms in a two formula unit $C2/m$ symmetry phase and an $I4/mmm$ structure were all octahedrally coordinated by four phosphorus atoms in the equatorial positions and two hydrogen atoms in the axial positions.

Isosurfaces of the electron localization function (ELF) confirmed covalent P-P and P-H bonding. The occupied bands were parabolic and the DOS nearly free electron like. As a result, these phases had a high DOS at E_F. A single point calculation on a geometry wherein the layers in $I4/mmm$-PH_2 were separated by about 10 Å showed that such a system would be a good metal, with a DOS at E_F slightly higher than that of the optimized phase. This computational experiment indicates that the metallicity is a result of the structure assumed by the two-dimensional sheet and that the mobile electrons move primarily within the 2D layers, and along the P-P bonds. It is likely that the metallicity within the other PH_n structures containing one-dimensional chains and two-dimensional sheets has the same origin.

Because a number of the dynamically stable PH_n phases gave rise to T_c values in-line with those found experimentally, the computations illustrate that the observed superconductivity is likely due to a mixture of metastable phases that form from the decomposition of phosphine under pressure. These studies also highlight that pressure can lead to the formation of (meta)stable phases with stoichiometries that are not observed at atmospheric conditions.

4 Characteristic Phonon Modes and Superconductivity

Structural characterization of the phases formed in diamond anvil cells can be quite challenging, especially for systems containing light elements. Often Raman or IR spectroscopy is utilized to monitor the behavior of select phonon modes as a function of pressure. By comparing the spectra with those of known structures one can determine if a new phase has been made. In addition, the experimental vibrational frequencies can be compared with those calculated for potential structural candidates via first principles. Importantly, because the hydrogenic motifs found in the polyhydrides give rise to characteristic vibrational modes, they can be used as spectroscopic fingerprints to aid in the identification of the species that are formed.

For example, the H_2 stretching mode is typically found between 3000-4500 cm^{-1}. Its frequency depends upon the H-H distance, with longer bonds yielding lower frequency vibrations. Both the pressure and the nature of the interaction between H_2 and the dopant element influence the bond strength. For example, in H_4I at 100 GPa the H–H distances measure 0.799 Å (as compared to the gas phase value of ∼0.75 Å) and the H_2 vibron peak is found at 3000-3300 cm^{-1}, as illustrated in Fig. 4(a). The weakening of the H–H bond is, at least in part, a result of electron transfer from iodine to H_2, which leads to a partial filling of the σ_u^*-levels.

The bending and asymmetric/symmetric stretching modes of the H_3^- motif are located between 1500-2500 cm^{-1}, and their frequency also depends upon the H–H distances. The symmetric vibration typically has a higher frequency. For example, in CsH_3 at 50 GPa it is centered around 2200 cm^{-1}, whereas modes associated with the asymmetric stretch are near 1700 cm^{-1}, as shown in Fig. 4(b).

Phases that contain extended hydrogenic lattices only, whether they be three-dimensional as in CaH_6 or one-dimensional as in SrH_6, do not exhibit any vibrations past ∼2250 cm^{-1}. This is evident in, the phonon DOS calculated for SrH_6 at 250 GPa in Fig. 4(c).

In the phosphorus polyhydrides above 100 GPa, hydrogen bonds covalently to phosphorus and the aforementioned hydrogenic motifs are absent. For the PH_n phases with $n = 1 - 3$ at 200 GPa the P-H stretching mode was found between 1800-2500 cm^{-1} [57–59]; for example see the phonon DOS for 2FU-$C2/m$ PH_2 in Fig. 4(d). The frequencies of X-H vibrations will depend on the pressure and the identity of element X, but they will be found at values lower than that of the hydrogen vibron due to the heavier mass of the dopant element.

Table 1 provides the electron-phonon coupling (EPC) parameter, λ, the logarithmic average frequency, $\omega_{\log}$, and the calculated T_c of various alkali metal and alkaline earth polyhydrides, YH_6, $Im\bar{3}m$-H_3S, as well as the aforementioned H_2I, H_4I, PH, PH_2 and PH_3 phases. The data has

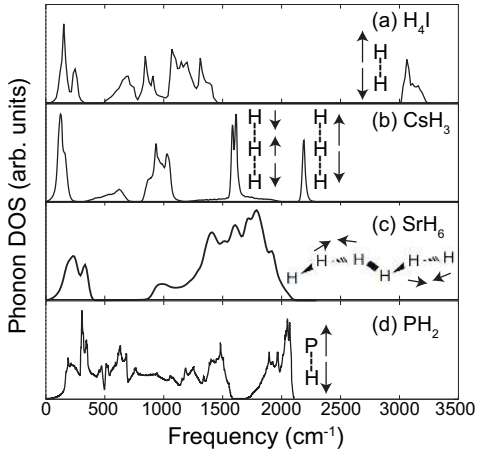

Figure 4: Phonon densities of states of (a) $P6/mmm$-H_4I, (b) $Cmmm$-CsH_3, (c) $R\bar{3}m$-SrH_6 and (d) 2FU-$C2/m$ PH_2 phases at 150, 50, 250, and 200 GPa, respectively. The hydrogenic structural motifs found in these phases are (a) molecular hydrogen with H–H distances of 0.799 Å, (b) H_3^- with H–H distances of 0.962 Å, (c) one-dimensional hydrogenic chains with H-H distances of 1.033 Å and (d) covalent P–H bonds with distances of 1.434-1.439 Å.

been organized loosely according to the structural motifs that are present in the hydrogenic lattices, and, in part, the computed λ. Most studies employed the Allen-Dynes modified McMillan equation [66] to estimate the superconducting critical temperature. The Coulomb pseudopotential, $\mu^\star$, was typically chosen to fall within 0.1 to 0.13. Because we would like to gain a better understanding of how the structural motifs present within the polyhydrides, and the mechanisms by which they become metallic influence T_c, data is provided for a uniform value of $\mu^\star = 0.1$. The only exception are the results from Ref. [58], wherein density functional theory for superconductors (SCDFT) was employed to calculate T_c for the PH_n phases.

Generally speaking, T_c was higher for the alkali metal and alkaline earth polyhydrides than for the polyhydrides of iodine, whose metallicity arises from their monoatomic iodine lattices. LiH_2, which did not superconduct at 150 GPa, was the only exception. This phase becomes metallic due to pressure induced broadening and overlap of the H^- and H_2 $\sigma_u^\star$-bands. However, at this pressure the Li 1s cores overlap so the valence electrons are impelled into interstitial regions thereby reducing the metallicity of LiH_2. MgH_4 and BaH_6 also contained H_2 and H^- units, so they metalized via the same mechanism as LiH_2. But, the EPC parameters, and therefore T_cs, of MgH_4 and BaH_6 were significantly higher than those of LiH_2. The superconducting critical temperatures of phases containing H_3^- motifs have not yet been calculated, but we suspect they may be somewhat lower than those of MgH_4 and BaH_6 because the H_3^- stretching modes occur at lower frequencies than the vibration of H_2, but the two classes of structures have a similar DOS at E_F.

The EPC parameters of phases that become metallic because of partial filling of the H_2 $\sigma_u^\star$-bands, such as LiH_6, LiH_8 and MgH_{12}, ranged from 0.6-0.9 and their T_cs fell between 47 K to 70 K (for the pressures listed herein). In comparison, the T_cs of MgH_4 and BaH_6 were somewhat lower, and this is primarily a result of their smaller $\omega_{\log}$ values. The largest contribution to λ in phases that metallize via partial filling of the H_2 $\sigma_u^\star$-bands or the overlap of the H^- and H_2 $\sigma_u^\star$-levels was due to vibrations of the hydrogen and dopant atoms.

T_c is pressure dependent; for example it is predicted to range from 38-82 K for LiH_6 between 150 and 300 GPa [24]. Calculations of the electronic structure of sulfur hydrides as a function of pressure have reported the presence of electronic topological transitions (ETT) at critical values of the pressure. At the ETT the chemical potential will be close to a band edge resulting in the appearance of a new Fermi surface with a small local Fermi energy [2]. These k-spots could be relevant for the scenario of multiband superconductivity in hydrides proposed by some authors [54, 55]. However, based on the trends observed so far it is unlikely that phases which metallize via the first or third mechanism described in Sec. 2, or the first mechanism outlined in Sec. 3, will be able to attain T_c values significantly higher than the boiling point of liquid nitrogen at any pressure.

Comparison of the results obtained for the hydrides of phosphorus with the alkali metal and alkali earth polyhydrides that contained H^- and/or $H_2^{\delta-}$ motifs revealed that the PH_n phases had a slightly higher λ, which ranged from 1.0-1.46 but their $\omega_{\log}$ were generally smaller. The vibrational modes that furnished the main contribution to the EPC parameter consisted of the motions of the phosphorus and hydrogen atoms. The computed T_cs of the PH_n phases fell between 30-80 K in the range of 100-250 GPa, and in general they increased with increasing pressure [58], in agreement with experimental observations [39].

The phases that had the highest T_c values were comprised of three-dimensional hydrogenic lattices. In fact, the calculated T_c of CaH_6, MgH_6 and YH_6 wherein the hydrogenic lattice resembled that of the sodalite clathrate rivaled that of the $Im\bar{3}m$-H_3S phase at 200 GPa. The reason why the former had a higher critical superconducting temperature than the latter was because of the larger EPC parameter, which ranged from 2.69-3.29 for the sodalite-like phases, as compared to 2.19 for H_3S. The T_c of a $R\bar{3}m$ SrH_6 phase that contained one-dimensional hydrogenic helices was not calculated [23, 32], but we expect it to be high be-

Table 1: The electron-phonon coupling parameter (λ), logarithmic average phonon frequency (ω_{log}) and computed superconducting transition temperature (T_c) calculated for $\mu^* = 0.1$ (except for Ref. 58) of various polyhydrides at select pressures. The motifs present in the hydrogenic lattices are also provided.

System	Pressure (GPa)	λ	ω_{log} (K)	T_c (K)	Hydrogenic Motifs
$Cmcm$-H_2I[a]	100	0.51	608.7	7.8	$H_2^{\delta-}$
H_4I[a]	150	0.56	1097.4	20.4	$H_2^{\delta-}$
$Pnma$-H_2I[b]	100	0.47	552.6	5.3	$H_2^{\delta-}$
$R\bar{3}m$-H_2I[b]	300	0.55	1465.8	25.1	$H^{\delta-}$
H_4I[b]	200	0.48	960.4	9.6	$H_2^{\delta-}$
LiH_2[c]	150	0.09	1740.8	0.0	H^-, H_2
MgH_4[d]	100	0.74	941.0	37.0	H^-, H_2
BaH_6[e]	100	0.77	878.0	38.0	$H_2^{\delta-}$, H^-
LiH_6[c]	150	0.64	1911.9	52.4	$H_2^{\delta-}$
LiH_6[*,c]	200	0.65	1952.7	55.9	$H_2^{\delta-}$
LiH_8[*,c]	150	0.64	1708.3	47.0	$H_2^{\delta-}$
LiH_8[*,c]	200	0.65	1754.5	49.7	$H_2^{\delta-}$
MgH_{12}[d]	140	0.73	1554.0	60.0	$H_2^{\delta-}$
KH_6[f]	166	0.91	1164.7	69.6	$H_2^{\delta-}$
5FU-$C2/m$ PH_2[g]	150	1.00	798.1	55.5	P-H
2FU-$C2/m$ PH_2[g]	200	1.04	1026.5	75.6	P-H
$I4/mmm$-PH_2[g]	200	1.13	851.6	70.4	P-H
PH_1[*,†,h]	200	1.29	679.5	61.5	P-H
PH_1[*,†,h]	250	1.42	816.7	82.7	P-H
PH_2[*,†,h]	180	1.18	720.2	61.0	P-H
PH_2[*,†,h]	220	1.35	763.6	78.0	P-H
PH_3[*,†,h]	180	1.00	884.0	50.5	P-H
PH_3[*,†,h]	220	1.09	734.4	55.7	P-H
PH_3[*,i]	200	1.46	826.0	91.7	P-H
$Im\bar{3}m$-SH_3[m]	200	2.19	1334.6	204.0	atomistic (S-H-S)
MgH_6[k]	300	3.29	1450.0	271.0	3-D
CaH_6[†,j]	150	2.69	-	235.0	3-D
YH_6[l]	120	2.93	-	264.0	3-D

[*]These values are estimates; they were taken from plots found in the original papers. [†]T_c was predicted using SCDFT (Ref. 58) or solving the Eliashberg equations numerically (Ref. 22). [a] Ref. 35, [b] Ref. 36, [c] Ref. 24, [d] Ref. 30, [e] Ref. 31, [f] Ref. 25, [g] Ref. 57, [h] Ref. 58, [i] Ref. 59, [j] Ref. 22, [k] Ref. 34 [l] Ref. 61, [m] Ref. 40.

cause the structure can be derived via a slight distortion of CaH_6.

The trends that emerge from this data suggest that the phases with the highest propensity for superconductivity do not contain any molecular hydrogen. They are either comprised of atomistic hydrogen stabilized by bonding to a main group element as in H_3S [43], or of extended hydrogenic lattices as in MgH_6, CaH_6, SrH_6 and YH_6. In comparison, the phases that metalized either via pressure induced band gap closure of the H^- and H_2 σ_u^*-bands, or via partial filling of the H_2 σ_u^*-bands had significantly smaller EPC parameters and concomitantly lower T_cs. Finally, phases whose metallicity originated from their non-hydrogenic lattices, for example H_nI, had among the lowest T_cs.

5 Conclusions

First principles calculations have been carried out to study the phase diagrams, as a function of composition and pressure, of a wide variety of hydrides. A number of phases with unique stoichiometries that contain either $H_2^{\delta-}$, H^-, H_3^-, extended hydrogenic lattices, or atomistic hydrogen stabilized by bonding to another element have been predicted to become stable at pressures accessible within diamond anvil cells. The mechanism by which these phases become metallic include: chemical and Madelung precompression, pressure induced broadening and overlap of H^- and H_2 σ^*-bands or the overlap of the H_3^- non-bonding and anti-bonding bands, partial filling of the H_2 σ^*-bands, met-

allization of non-hydrogenic sublattices, or simply by the presence of extended hydrogenic motifs and the absence of molecular ones.

The phases which had the highest estimated superconducting critical temperatures did not contain discrete hydrogenic units such as H^-, $H_2^{\delta-}$ or H_3^-. Instead, they were comprised of extended hydrogenic lattices such as those found in MgH_6, CaH_6, SrH_6, and YH_6, or atomistic hydrogen stabilized by bonding to a *p*-group element such as in H_3S or PH_n, $n = 1, 2, 3$. Importantly, comparison of the theoretical [57–59] and experimental [39] studies of the polyhydrides of phosphorus revealed that metastable phases may be made experimentally and that superconductivity can result from a mixture of phases. Thus, theoretical studies should not only focus on examining the properties of those systems that are thermodynamically stable, but also on searching for metastable phases with the aforementioned hydrogenic lattices that are conducive for high-temperature superconductivity.

Acknowledgement: E.Z. acknowledges the NSF (DMR-1505817) for financial support. A.S. acknowledges financial support from the Department of Energy National Nuclear Security Administration under Award Number DE-NA0002006. We also thank the Center for Computational Research (CCR) at SUNY Buffalo for computational support.

References

[1] N. W. Ashcroft. Hydrogen Dominant Metallic Alloys: High Temperature Superconductors? *Phys. Rev. Lett.* 92, 2004, 187002 (1–4).

[2] N. W. Ashcroft. Symmetry and Heterogeneity in High Temperature Superconductors. *NATO Science Series II: Mathematics, Physics and Chemistry* 214, 3-20, 2006.

[3] J. Feng, W. Grochala, T. Jaron, R. Hoffmann, A. Bergara, and N. W. Ashcroft. Structures and Potential Superconductivity in SiH_4 at High Pressure: En Route to Metallic Hydrogen. *Phys. Rev. Lett.* 96, 2006, 017006 (1–4).

[4] C. J. Pickard and R. J. Needs. High–Pressure Phases of Silane. *Phys. Rev. Lett.* 97, 2006, 045504 (1–4).

[5] O. Degtyareva, M. M. Canales, A. Bergara, X. Chen, Y. Song, V. V. Struzhkin, H. Mao, and R. J. Hemley. Crystal Structure of SiH_4 at High Pressure. *Phys. Rev. B* 76, 2007, 064123 (1–4).

[6] Y. Yao, J. S. Tse, Y. Ma, and K. Tanaka. Superconductivity in High–Pressure SiH_4. *EPL* 78, 2007, 37003 (1–6).

[7] H. Zhang, X. Jin, Y. Lv, Q. Zhuang, Y. Liu, Q. Lv, K. Bao, D. Li, B. Liu, and T. Cui. High–Temperature Superconductivity in Compressed Solid Silane. *Sci. Rep.* 5, 2015, 8845 (1–7).

[8] M. Martinez-Canales, A. R. Oganov, Y. Ma, Y. Yan, A. O. Lyakhov, and A. Bergara. Novel Structures and Superconductivity of Silane Under Pressure. *Phys. Rev. Lett.* 102, 2009, 087005 (1–4).

[9] Y. Yao and D. D. Klug. Silane Plus Molecular Hydrogen as a Possible Pathway to Metallic Hydrogen. *Proc. Natl. Acad. Sci. USA* 107, 2010, 20893–20898.

[10] M. I. Eremets, I. A. Trojan, S. A. Medvedev, J. S. Tse, and Y. Yao. Superconductivity in Hydrogen Dominant Materials: Silane. *Science* 319, 2008, 1506–1509.

[11] M. Martinez-Canales, A. Bergara, J. Feng, and W. Grochala. Pressure Induced Metallization of Germane. *J. Phys. Chem. Solids* 67, 2006, 2095–2099.

[12] G. Gao, A. R. Oganov, A. Bergara, M. Martinez-Canales, T. Cui, T. Iitaka, Y. Ma, and G. Zou. Superconducting High Pressure Phase of Germane. *Phys. Rev. Lett.* 101, 2008, 107002 (1–4).

[13] G. Zhong, C. Zhang, X. Chen, Y. Li, R. Zhang, and H. Lin. Structural, Electronic, Dynamical, and Superconducting Properties in Dense $GeH_4(H_2)_2$. *J. Phys. Chem. C* 116, 2012, 5225–5234.

[14] R. Szczesniak, A. P. Durajski, and D. Szczesniak. Study of the Superconducting State in the *Cmmm* Phase of GeH_4 Compound. *Solid State Commun.* 165, 2013, 39–44.

[15] C. J. Pickard and R. J. Needs. Metallization of Aluminum Hydride at High Pressures: A First–Principles Study. *Phys. Rev. B* 76, 2007, 144114 (1–5).

[16] I. Goncharenko, M. I. Eremets, M. Hanfland, J. S. Tse, M. Amboage, Y. Yao, and I. A. Trojan. Pressure–Induced Hydrogen–Dominant Metallic State in Aluminum Hydride. *Phys. Rev. Lett.* 100, 2008, 045504 (1–4).

[17] M. Geshi and T. Fukazawa. Pressure Induced Band Gap Opening of AlH_3. *Physica B: Condensed Matter* 411, 2013, 154–160.

[18] A. E. Carlsson and N. W. Ashcroft. Approaches for Reducing the Insulator-Metal Transition Pressure in Hydrogen. *Phys. Rev. Lett.* 50, 1983, 1305–1308.

[19] E. Zurek, R. Hoffmann, N. W. Ashcroft, A. R. Oganov, and A. O. Lyakhov. A Little Bit of Lithium Does a Lot for Hydrogen. *Proc. Natl. Acad. Sci.* 106, 2009, 17640–17643.

[20] C. J. Pickard and R. J. Needs. Ab Initio Random Structure Searching. *J. Phys.: Condens. Matter* 23, 2011, 053201.

[21] V. V. Struzhkin, D. Y. Kim, E. Stavrou, T. Muramatsu, H. Mao, C. J. Pickard, R. J. Needs, V. B. Prakapenka, and A. F. Goncharov. Synthesis of Sodium Polyhydrides at High Pressures. *Nat. Commun.* 7, 2016, 12267.

[22] H. Wang, J. S. Tse, K. Tanaka, T. Iitaka, and Y. Ma. Superconductive Sodalite–Like Clathrate Calcium Hydride at High Pressures. *Proc. Natl. Acad. Sci. USA* 109, 2012, 6463–6466.

[23] Y. Wang, H. Wang, J. S. Tse, T. Iitaka, and Y. Ma. Structural Morphologies of High–Pressure Polymorphs of Strontium Hydrides. *Phys. Chem. Chem. Phys.* 17, 2015, 19379–19385.

[24] Y. Xie, Q. Li, A. R. Oganov, and H. Wang. Superconductivity of Lithium–Doped Hydrogen Under Pressure. *Acta Cryst. C* 70, 2014, 104–111.

[25] D. Zhou, X. Jin, X. Meng, G. Bao, Y. Ma, B. Liu, and T. Cui. Ab Initio Study Revealing a Layered Structure in Hydrogen–Rich KH_6 Under High Pressure. *Phys. Rev. B* 86, 2012, 014118 (1–7).

[26] P. Baettig and E. Zurek. Pressure–Stabilized Sodium Polyhydrides: NaH_n ($n > 1$). *Phys. Rev. Lett.* 106, 2011, 237002 (1–4).

[27] J. Hooper and E. Zurek. Rubidium Polyhydrides Under Pressure: Emergence of the Linear H_3^- Species. *Chem–Eur. J.* 18, 2012, 5013–5021.

[28] J. Hooper and E. Zurek. High Pressure Potassium Polyhydrides: A Chemical Perspective. *J. Phys. Chem. C* 116, 2012, 13322–13328.

[29] A. Shamp, J. Hooper, and E. Zurek. Compressed Cesium Polyhydrides: Cs^+ Sublattices and H_3^- Three-Connected Nets. *Inorg. Chem.* 51, 2012, 9333–9342.

[30] D. C. Lonie, J. Hooper, B. Altintas, and E. Zurek. Metallization of Magnesium Polyhydrides Under Pressure. *Phys. Rev. B* 87, 2013, 054107 (1–8).

[31] J. Hooper, B. Altintas, A. Shamp, and E. Zurek. Polyhydrides of the Alkaline Earth Metals: A Look at the Extremes Under Pressure. *J. Phys. Chem. C* 117, 2013, 2982–2992.

[32] J. Hooper, T. Terpstra, A. Shamp, and E. Zurek. Composition and Constitution of Compressed Strontium Polyhydrides. *J. Phys. Chem. C* 118, 2014, 6433–6447.

[33] (E. Zurek. Hydrides of the Alkali Metals and Alkaline Earth Metals Under Pressure. *Comments Inorg. Chem.*, Submitted for Publication.)

[34] X. Feng, J. Zhang, G. Gao, H. Liu, and H. Wang. Compressed Sodalite–Like MgH_6 as a Potential High-Temperature Superconductor. *RSC Adv.* 5, 2015, 59292–59296.

[35] A. Shamp and E. Zurek. Superconducting High-Pressure Phases Composed of Hydrogen and Iodine. *J. Phys. Chem. Lett.* 6, 2015, 4067–4072.

[36] D. Duan, F. Tian, Y. Liu, X. Huang, D. Li, H. Yu, Y. Ma, B. Liu, and T. Cui. Enchancement of T_c in the Atomic Phase of Iodine–Doped Hydrogen at High Pressures. *Phys. Chem. Chem. Phys* 17, 2015, 32335–32340.

[37] C. Pépin, P. Loubeyre, F. Occelli, and P. Dumas. Synthesis of Lithium Polyhydrides Above 130 GPa at 300 K. *Proc. Natl. Acad. Sci.* 112, 2015, 7673–7676.

[38] A. P. Drozdov, M. I. Eremets, I. A. Troyan, V. Ksenofontov, and S. I. Shylin. Conventional Superconductivity at 203 Kelvin at High Pressures in the Sulfur Hydride System. *Nature* 525, 2015, 73–76.

[39] A. P. Drozdov, M. I. Eremets, and I. A Troyan. Superconductivity Above 100 K in PH_3 at High Pressures. arXiv:1508.06224.

[40] D. Duan, Y. Liu, F. Tian, D. Li, X. Huang, Z. Zhao, H. Yu, B. Liu, W. Tian, and T. Cui. Pressure–Induced Metallization of Dense $(H_2S)_2H_2$ with High-T_c Superconductivity. *Sci. Rep.* 4, 2014, 6968 (1–6).

[41] Y. Li, L. Wang, H. Liu, Y. Zhang, J. Hao, C. J. Pickard, J. R. Nelson, R. J. Needs, W. Li, Y. Huang, I. Errea, M. Calandra, F. Mauri, and Y. Ma. Dissociation Products and Structures of Solid H_2S at Strong Compression. *Phys. Rev. B* 93, 2016, 020103.

[42] J. A. Flores-Livas, A. Sanna, and E. K. U. Gross. High Temperature Superconductivity in Sulfur and Selenium Hydrides at High Pressure. *Eur. Phys. J. B* 89, 2016, 63.

[43] D. A. Papaconstantopoulos, B. M. Klein, M. J. Mehl, and W. E. Pickett. Cubic H_3S Around 200 GPa: An Atomic Hydrogen Superconductor Stabilized by Sulfur. *Phys. Rev. B* 91, 2015, 184511.

[44] N. Bernstein, C. S. Hellberg, M. D. Johannes, I. I. Mazin, and M. J. Mehl. What Superconducts in Sulfur Hydrides Under Pressure and Why? *Phys. Rev. B* 91, 2015, 060511.

[45] D. Duan, X. Huang, F. Tian, D. Li, H. Yu, Y. Liu, Y. Ma, B. Liu, and T. Cui. Pressure–Induced Decomposition of Solid Hydrogen Sulfide. *Phys. Rev. B* 91, 2015, 180502.

[46] I. Errea, M. Calandra, C. J. Pickard, J. Nelson, R. J. Needs, Y. Li, H. Liu, Y. Zhang, Y. Ma, and F. Mauri. High–Pressure Hydrogen Sulfide from First–Principles: A Strongly Anharmonic Phonon–Mediated Superconductor. *Phys. Rev. Lett.* 114, 2015, 157004 (1–5).

[47] R. Akashi, M. Kawamura, S. Tsuneyuki, Y. Nomura, and R. Arita. First–Principles Study of the Pressure and Crystal–Structure Dependences of the Superconducting Transition Temperature in Compressed Sulfur Hydrides. *Phys. Rev. B* 91, 2015, 224513.

[48] I. Errea, M. Calandra, C. J. Pickard, J. R. Nelson, R. J. Needs, Y. Li, H. Liu, Y. Zhang, Y. Ma, and F. Mauri. Quantum Hydrogen–Bond Symmetrization in the Superconducting Hydrogen Sulfide System. *Nature* 532, 2016, 81–84.

[49] Y. Quan and W. E. Pickett. Van Hove Singularities and Spectral Smearing in High–Temperature Superconducting H_3S. *Phys. Rev. B* 93, 2016, 104526.

[50] W. Sano, T. Koretsune, T. Tadano, R. Akashi, and R. Arita. Effect of Van Hove Singularities on High-T_c Superconductivity in H_3S. *Phys. Rev. B* 93, 2016, 094525.

[51] L. Ortenzi, E. Cappelluti, and L. Pietronero. Band Structure and Electron–Phonon Coupling in H_3S: A Tight–Binding Model. *Phys. Rev. B* 94, 2016, 064507.

[52] L. P. Gorkov and V. Z. Kresin. Pressure and High-T_c Superconductivity in Sulfur Hydrides. *Sci. Rep.* 6, 2016, 25608.

[53] A. F. Goncharov, S. S. Lobanov, I. Kruglov, X. Zhao, X. Chen, A. R. Oganov, Z. Konopkova, and V. B. Prakapenka. Hydrogen Sulfide at High Pressure: Change in Stoichiometry. *Phys. Rev. B* 93, 2016, 174105.

[54] A. Bianconi, and T. Jarlborg. Superconductivity Above the Lowest Earth Temperature in Pressurized Sulfur Hydride. *EPL* 112, 2015, 37001.

[55] T. Jarlborg, and A. Bianconi. Breadown of the Migdal Approximation at Lifshitz Transitions with Giant Zero-Point Motion in the H_3S Superconductor. *Sci. Rep.* 6, 2016, 24816.

[56] M. Einaga, M. Sakata, T. Ishikawa, K. Shimizu, M. I. Eremets, A. P. Drozdov, I. A. Troyan, N. Hirao, and Y. Ohishi. Crystal Structure of the Superconducting Phase of Sulfur Hydride. *Nat. Phys.* 12, 2016, 835–838.

[57] A. Shamp, T. Terpstra, T. Bi, Z. Falls, P. Avery, and E. Zurek. Decomposition Products of Phosphine Under Pressure: PH_2 Stable and Superconducting? *J. Am. Chem. Soc.* 138, 2016, 1884–1892.

[58] J. A. Flores-Livas, M. Amsler, C. Heil, A. Sanna, L. Boeri, G. Profeta, C. Wolverton, S. Goedecker, and E. K. U. Gross. Superconductivity in Metastable Phases of Phosphorus–Hydride Compounds Under High Pressure. *Phys. Rev. B* 93, 2016, 020508(R) 1–6.

[59] H. Liu, Y. Li, G. Gao, J. S. Tse, and I. I. Naumov. Crystal Structure and Superconductivity of PH_3 at High Pressures. *J. Phys. Chem. C* 120, 2016, 3458–3461.

[60] M. Ayouz, O. Dulieu, R. Guerout, J. Robert, and V. Kokoouline. Potential Energy and Dipole Moment Surfaces of H_3^- Molecule. *J. Chem. Phys.* 132, 2010, 194309 (1–11).

[61] Y. Li, J. Hao, H. Liu, J. S. Tse, Y. Wang, and Y. Ma. Pressure–Stabilized Superconductive Yttrium Hydrides. *Sci. Rep.* 5, 2015, 9948.

[62] L. Zhang, Y. Wang, X. Zhang, and Y. Ma. High–Pressure Phase Transitions of Solid HF, HCl and HBr: An Ab Initio Evolutionary Study. *Phys. Rev. B* 82, 2010, 014108 (1–8).

[63] J. V. Straaten and I. F. Silvera. Observation of Metal–Insulator and Metal–Metal Transitions in Hydrogen Iodide Under Pressure. *Phys. Rev. Lett* 57, 1986, 766–770.

[64] B. M. Riggleman and H. G. Drickamer. Approach to the Metallic State as Obtained from Optical and Electrical Measurments. *J. Chem. Phys.* 38, 1963, 2721.

[65] T. Kenichi, S. Kyoko, F. Hiroshi, and O. Mitsuko. Modulated Structure of Solid Iodine During Its Molecular Dissociation Under High Pressure. *Nature* 423, 2003, 971–974.

[66] P. B. Allen and R. C. Dynes. Transition Temperature of Strong–Coupled Superconductors Reanalyzed. *Phys. Rev. B* 12, 1975, 905–922.